

Many-Body Correlation Effects on the x_{Bjorken} -Dependence of Cross Section Ratios off Nuclei for $1 < x_{\text{Bjorken}} < 2$

Athanasios Petridis, Allen Barr, Drew Fustin

Department of Physics and Astronomy, Drake University, Des Moines, USA

Email: athan.petridis@drake.edu

How to cite this paper: Petridis, A., Barr, A. and Fustin, D. (2022) Many-Body Correlation Effects on the x_{Bjorken} -Dependence of Cross Section Ratios off Nuclei for $1 < x_{\text{Bjorken}} < 2$. *Journal of Modern Physics*, 13, 46-65.

<https://doi.org/10.4236/jmp.2022.131004>

Received: July 17, 2020

Accepted: January 17, 2022

Published: January 20, 2022

Copyright © 2022 by author(s) and Scientific Research Publishing Inc. This work is licensed under the Creative Commons Attribution International License (CC BY 4.0).

<http://creativecommons.org/licenses/by/4.0/>



Open Access

Abstract

Many-body correlations in nuclei determine the behavior of Deep-Inelastic-Scattering (DIS) and Quasi-Elastic Scattering (QES) cross section ratios off heavy over light nuclei especially for $x_{\text{Bjorken}} > 1$, obtained at Jefferson Lab. They can be described in terms of quark-cluster formation in nuclei due to wave-function overlapping, manifesting itself when the momentum transfer is high so that the partonic degrees of freedom are resolved. In clusters (correlated nucleons) the quark and gluon momentum distributions are softer than in single nucleons and extend to $x_{\text{Bjorken}} > 1$. The cluster formation probabilities are computed using a network-defining algorithm in which the initial nucleon density is either standard Woods-Saxon or is input from lower energy data while the critical radius for nucleon merging is an adjustable parameter. The exact choice of critical radius depends on the specific nucleus and it is anti-correlated to the rescaling of the x_{Bjorken} needed for bound nucleons. The calculations show that there is a strong dependence of the cross section ratios on the x_{Bjorken} in agreement with the data and that four-body correlations are needed to explain the experimental results even in the range $1 < x_{\text{Bjorken}} < 2$. The dependence on the specific exponents of parton distributions in high-order clusters is weak.

Keywords

Deep Inelastic Scattering, Quasi-Elastic Scattering, Short-Range Correlations, Quark-Clusters

1. Introduction

The atomic nucleus is typically described as a system of protons and neutrons

interacting via some potential that binds them together. Pions emerge as the quanta of these interactions. When the nucleus is probed by high-energy projectiles the parton-degrees of freedom of the nucleons and the pions are resolved and the picture of the quark model emerges. In this energy region the quarks appear to interact among themselves by means of gluons which in turn can give rise to quark-antiquark pairs, constituting the sea or ocean inside the nucleons and are distinguished from the valence quarks that make up the “core” of each nucleon. However, it is usually assumed that no matter how complicated the interactions among nucleons are or how high the energy scale of the probe is, the nucleons maintain their individuality and independence from one another, *i.e.*, they are uncorrelated. Data accumulated over the past two decades strongly suggest that this picture is overly simplistic.

The so called EMC-effect, named after the European Muon Collaboration [1] [2] [3] [4] [5], has shown that in the case of Deep Inelastic Scattering (DIS) of muons off nuclei the cross section does not scale with the number of nucleons and exhibits a strong dependence on the longitudinal momentum fraction carried by the struck quarks. This effect has been observed in many other processes involving the electromagnetic and the weak interactions of nuclei with probes at high energies, such as Drell-Yan pair production, neutrino scattering, and charmonium and bottomonium suppression [6] [7] [8] [9] [10] and predicted for direct photon production in hadron-nucleus and nucleus-nucleus collisions [11] [12] [13].

The many-body correlations can be attributed to a physical overlap of the bound nucleons leading to the formation of multi-quark clusters and the consequent exchange of quarks and gluons that results in softening of the parton distributions. The concept of multi-quark clusters was originally proposed by Pirner, Vary and Coon [14] [15] [16] and has had significant success in interpreting data on a variety of processes involving hadron-nucleus and nucleus-nucleus collisions such as those mentioned above [17]-[23]. This is the approach taken in this work. A model that describes the probability for such overlaps is developed along with reasonable assumptions about the parton distributions in clusters. The authors of Ref [24] have addressed the issue of correlations by estimating their probability to be formed and comparing the results with heavy-to-light nuclei cross section ratios for Quasi-Elastic Scattering. These results are in general agreement with the data but do not describe the explicit dependence of those ratios on the momentum fraction of the struck parton. This dependence contains a wealth of information on the nature of the correlations and their effect on the parton momentum distributions.

This article is organized as follows: in Section 2, the concept of many-body correlations is introduced and described in terms of multi-quark clusters in the nucleus. In Section 3, a network-based algorithm for calculating cluster probabilities given an initial spatial distribution of nucleons is presented. Those probabilities are expressed as functions of a critical distance (radius) between two

nucleons. In Section 4, a method to calculate the numbers of various types of clusters (proton-proton, proton-neutron, etc.) in a given nucleus is introduced. In Section 5, the parton (quark and gluon) momentum distributions in clusters are postulated on the basis of existing data. They are expressed as functions of the longitudinal parton momentum fraction, x_{Bjorken} . In Section 6, it is argued that for bound nucleons, x_{Bjorken} may have to be rescaled by a multiplicative factor η . In Section 7, the structure functions of nuclei are calculated as sums of products of quark distributions weighted by the squares of the quark charges and summed over all types of clusters. In Section 8, the heavy-to-light nuclei cross section ratio is defined. In Section 9, comparison of the theoretical calculations with two sets of data is presented and the best-fit parameters (the critical radius and the rescaling factor) are extracted. The similarity of correlations between Deep Inelastic Scattering (DIS) and Quasi Elastic Scattering (QES) is discussed. Section 10 details the need for many-body correlations as indicated by data. Finally, in Section 11 conclusions are drawn and some directions of future continuation of this research are suggested.

2. Correlations as Quark-Clustering

Correlations among nucleons bound inside nuclei imply that the nucleons are not independent particles so that the nucleus is not a collection of mutually interacting, yet separate constituents. From a quantum-mechanical perspective this means that the wave-functions of nucleons overlap sufficiently to produce effective aggregates. These can be identified as clusters of various orders, from 1st-order, that is single nucleons, to 2nd-order, made of two nucleons and so on. When the protons and neutrons are so close together, they can easily exchange gluons and sea quarks. As the gluons propagate they can also produce quark-antiquark pairs which subsequently annihilate back into gluons. The quarks may emit and reabsorb gluons. The sharing of such particles leads to energy and momentum exchanges among the nucleons and modifications to the parton momentum distributions inside them.

In experiments using high energy electrons (or muons) as probes to peek into the structure of the nucleus the 4-momentum exchange between the projectile and the target determines the spatial and temporal resolution of the image of the nucleus and its constituents. When the square of the 4-momentum exchange, Q^2 , exceeds 2 GeV^2 the sub-nucleonic (parton) degrees of freedom start being resolved, *i.e.*, the interaction is directly between the electron and the quarks since the exchange photon wavelength is $\lambda = h/\sqrt{Q^2}$. This corresponds to distances just under 1 fm. Given the average nuclear density it is at this distance that nucleon wave-functions begin to overlap. Consequently, at relatively low Q^2 the electron interacts with quarks in single nucleons and at high Q^2 with quarks that may be shared among nucleons in clusters. This is illustrated in **Figure 1**. Furthermore, if the (invariant) photon energy, ν , is also large (greater than 1 GeV) the quarks are probed in the asymptotically free region, that is the strong interaction among them is greatly weakened and the cross section becomes

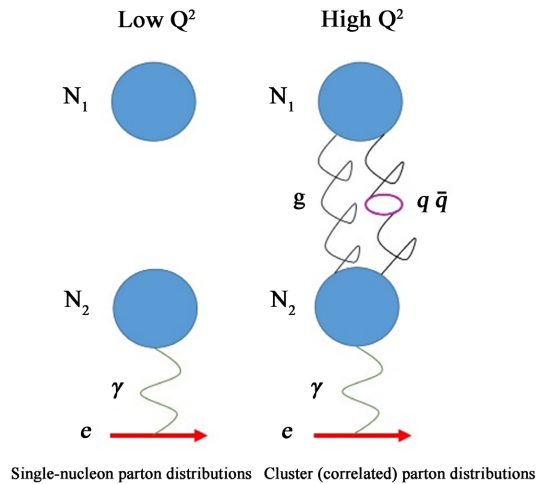


Figure 1. Electron scattering off nuclei. At low momentum transfer (low Q^2) the exchange photon resolves individual nuclei. As the momentum transfer increases the gluon (including quark-antiquark bubbles) exchange is probed. The nucleons are no longer independent and can be treated as clusters. The parton distributions in the clusters differ from those of single nucleons and become softer.

approximately independent of Q^2 , depending only on the invariant quantity $x_{\text{Bjorken}} = Q^2/2M\nu$, where M is the nucleon mass (the Bjorken- x scaling variable, which, in a frame of reference where the nucleons move very fast and the transverse momentum components can be neglected, is the longitudinal momentum fraction of a nucleon carried by a struck quark). This kinematic region is referred to as Deep Inelastic Scattering (DIS), while the region with large Q^2 and lower ν in which the quarks are not completely resolved, is known as the Quasi-Elastic Scattering (QES) region. Completely elastic scattering corresponds to $x_{\text{Bjorken}} = 1$. Nucleon binding and the resulting Fermi motion lead to smearing of the cross section allowing x_{Bjorken} to deviate from unity. It has been reasonably argued [8] that Fermi motion and the formation of clusters, *i.e.*, the presence of correlations among bound nucleons are strongly overlapping concepts.

3. Calculation of Clustering Probabilities

The probabilities for quark-cluster formation can be calculated using a quasi-classical network-based algorithm. An initial distribution of particles, nucleons in this case, is produced. The coordinates of these particles are determined randomly from the given distribution in 3 dimensions. Then the array of distances between the particles is computed. The algorithm determines the particles whose distances are smaller than a critical radius R_c relative to one another and assigns these particles to a particular network (cluster). Special care is taken to ensure that each particle belongs to one and only one cluster. The particles are not physically displaced so that the center of mass remains fixed. The algorithm then counts the clusters of each order, the total number of clusters and the fraction that corresponds to each order. The process is repeated many times starting from different randomly-generated initial coordinates. The final averaged num-

bers of fractions are reported as the probabilities for each cluster-order for the chosen critical radius. The latter is then incremented and the algorithm is rerun to finally obtain the probabilities as functions of R_c . Specifically, the algorithm for N particles consists of the following steps:

(1) A spherically-symmetric distribution of N particles (nucleons) is produced for a range of different R_c (critical distance) values using either a Woods-Saxon nuclear density or a Fourier-Bessel nuclear density, fit to real experimental data. The distance array $d(i, j)$ for $i, j = 1, \dots, N$ is produced holding the values for the distances between each of the N particles in the distribution. Then, the initial network array $A_0(i, j)$ for $i, j = 1, \dots, N$ is produced so that $A_0(i, j) = 1$ if $d(i, j) < R_c$ and $A_0(i, j) = 0$ otherwise. The initial network array is reduced to the final network array $A(i, j)$ for $i, j = 1, \dots, N$ in the following manner.

(2) Each column $i = 1, \dots, N - 1$ is compared with column $k = i + 1, \dots, N$.

(3) If two separate columns contain a 1 in the same position, the two columns are merged by replacing the column $A(i, j)$ with the result of $(A(i, j) \text{ OR } A(k, j))$ and the column $A(k, j)$ with the zero vector.

(4) The number of 1's in each column of the matrix $A(i, j)$ is then counted. This number corresponds to the order of the (quark) cluster that column is a part of. The total number of clusters of each order is then counted for the trial. These values are averaged over a large number of initial arrays for each R_c . The cluster probabilities f_m , where m is the order of the cluster, are the fractions of a cluster-type number over the total cluster number. The order m varies from 1 up to N .

The crucial steps in the above algorithm are (2) and (3). Step (2) ensures that all networks that are formed maintain their internal structure while step (3) guarantees that each particle is assigned to one and only one network, specifically the network from a member of which the said particle has the smallest distance. This step identifies all the networks upon cycling over the array of 1's and 0's that describe distances that pass the critical-radius test.

The initial particle distribution can be chosen to be a Woods-Saxon in the radial direction and uniform in the azimuthal and polar directions. Another option is to use a radial distribution derived from experimental data using a Fourier-Bessel method [25] [26]. In either case the results are consistent with larger cluster probabilities for larger and denser nuclei. In this approach the coalescence happens entirely in coordinate space. Even though the Fermi motion is implicit in the finite size of the wave-function, approximated by the critical radius, the relative momentum of the nucleons is not considered. Also differences between protons and neutrons are neglected at this stage. In **Figure 2** a schematic diagram of cluster formation is shown. In **Figure 3** the probabilities, f_m , for clusters of order $m = 1, \dots, N$ are plotted as functions of the critical radius R_c for various nuclei characterized by their mass number A which in this case is the total number of particles (N). The Woods-Saxon radial distribution is used, $P_r(r) \sim 1/\left[1 + \exp\left(\frac{r-a}{b}\right)\right]$, where r is the distance from the center of mass of

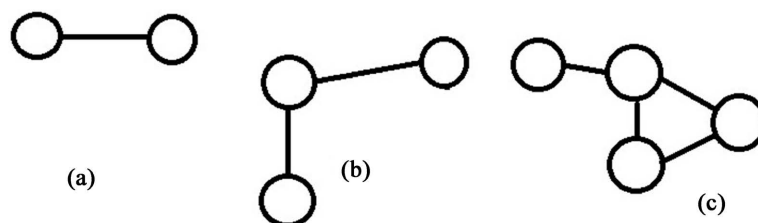


Figure 2. Three types of clusters produced by the network algorithm. (a) 2nd-order cluster (two nucleons or six valence quarks). (b) One type of 3rd-order cluster (three nucleons or nine valence quarks). (c) One type of 4th-order cluster (four nucleons or twelve valence quarks). The straight-line links indicate distances that are smaller than the critical radius.

the system, with an attenuation factor $b = 0.55$ fm and skin-thickness $a = 0.33$ fm. It is observed that as the critical radius increases larger clusters are favored, resulting in a non-monotonic behavior. In the case of $A = 12$ (carbon) results originating in a Fourier-Bessel initial radial distribution are shown for comparison (**Figure 4**). The difference in cluster probabilities between Woods-Saxon and Fourier-Bessel is small. For this work the Woods-Saxon distribution is used.

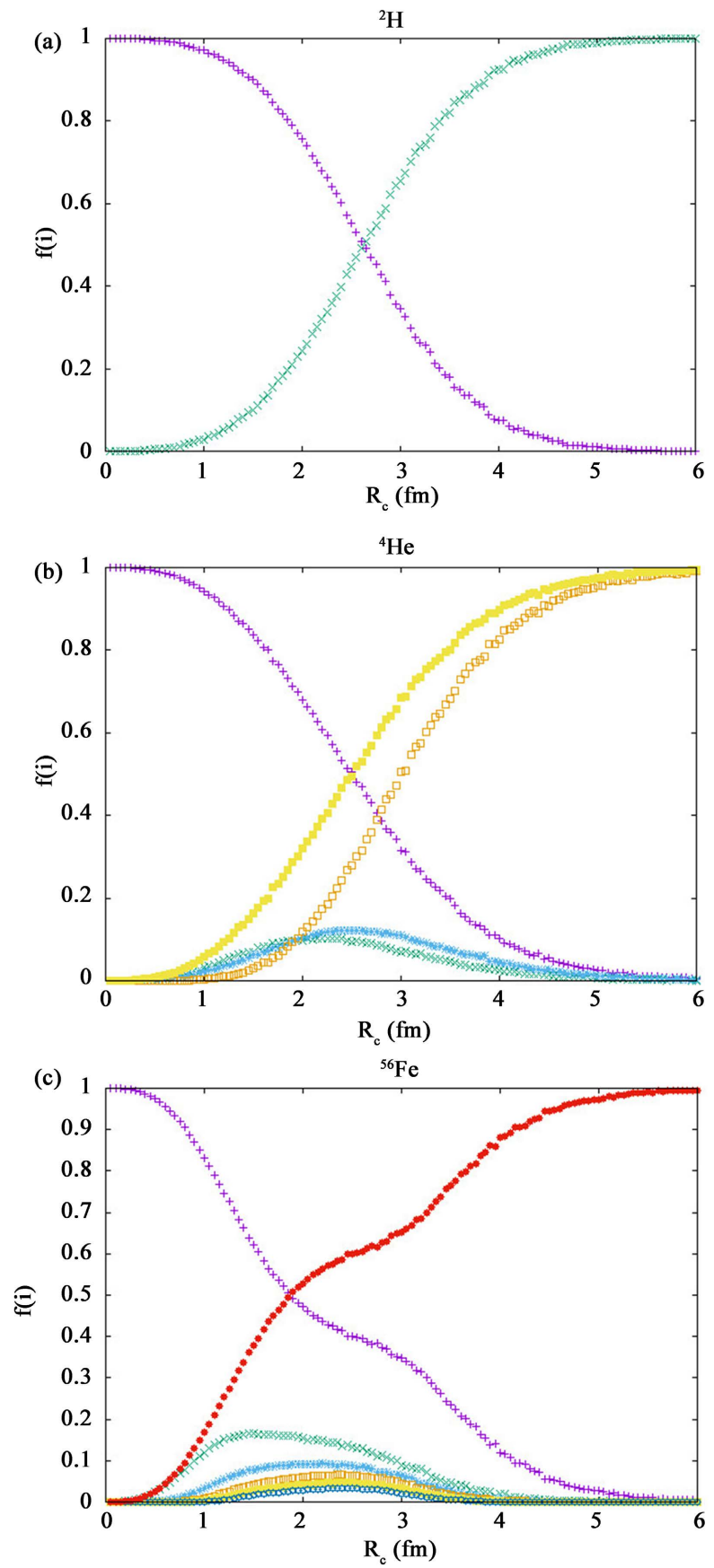
The free parameter in this calculation is the critical radius. This determines the relative values of cluster probabilities, hence the departure from single-nucleon physics. Earlier studies [7] [8] indicate that to account for diverse phenomena such as the EMC effect in DIS, nuclear, initial-state modifications of the Drell-Yan production, suppression of J/Ψ production in processes involving nuclei the cumulative cluster probability for deuterium should be about 4% and for heavy nuclei it could exceed 30% (**Table 1**). The approximate dependence of the cumulative probability on the mass number is logarithmic but for magic or doubly-magic nuclei this probability is higher. In practice, the critical radius will be treated as a parameter to be estimated using particle scattering data off nuclei.

It must be pointed out that the algorithm described in this section does not physically replace nucleons with a single object at the center of mass of the cluster while it is still running. It simply identifies networks of nucleons without changing the spatial distribution of matter (and charge) or moving the center of mass of the system.

4. Types of Clusters in Nuclei

The parton distributions in clusters depend on the type of valance quarks in the nucleons they are made of. The 2nd-order clusters may consist of two protons (pp-type), two neutrons (nn-type) or a proton and a neutron (np-type). The 3rd-order clusters can be of nnn, ppp, npp or nnp-type. A similar designation can be assigned to higher-order clusters. Therefore, a model is needed in order to calculate how many clusters of each type are present in a given nucleus at each value of the critical radius.

To derive the cluster numbers for a nucleus of mass number A and atomic number Z certain constraints must apply. 1) The total mass of the nucleus must be fixed. In other words, the total baryon number of all clusters must remain



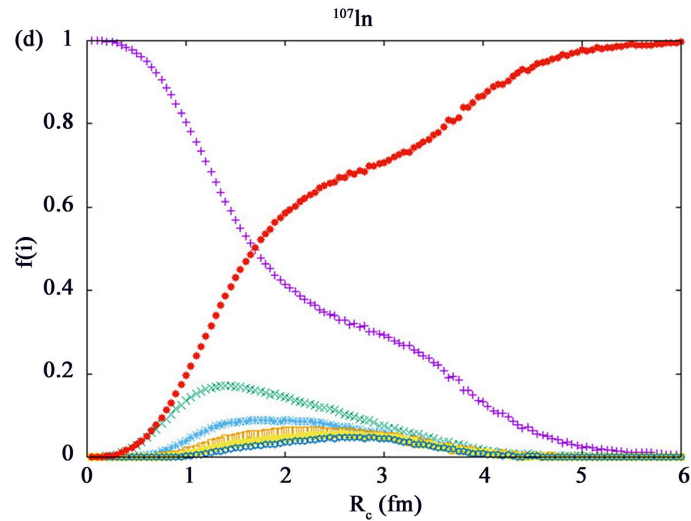


Figure 3. Cluster probabilities versus critical radius in fm. (a) $A = 2$. The brown points correspond to the two-nucleon cluster. (b) $A = 4$. The brown, green, black and purple points correspond to 1st, 2nd, 3rd and 4th-order clusters. The light-blue points indicate the cumulative cluster probability. (c) $A = 56$. The brown, green, dark-blue, purple and bright-green points correspond to 1st, 2nd, 3rd, 4th and 5th-order clusters. The black points indicate the cumulative cluster probability. (d) $A = 107$. The notation is the same as in the lower left panel. All these results are produced using Woods-Saxon radial probability density.

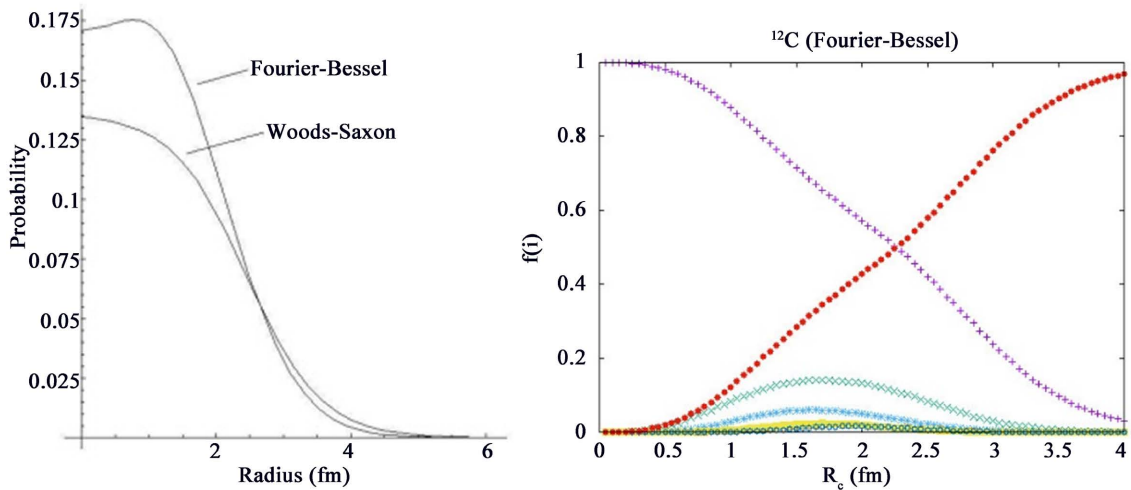


Figure 4. Left panel: the Woods-Saxon and the experimentally-derived Fourier-Bessel radial probability distributions versus the distance from the center of mass. For ^{12}C . Right panel: Cluster probabilities for ^{12}C versus the critical radius.

Table 1. A sample list of cumulative cluster probabilities for two values of the critical radius. For ^{12}C the results produced using Woods-Saxon (WS) and Fourier-Bessel radial distributions are shown for comparison. For ^{197}Au the probability can be more than 0.30.

Nucleus	Cluster Probability (f) for $R_c = 0.85$ fm	Cluster Probability (f) for $R_c = 0.85$ fm
^2H	0.04	0.09
^{12}C (WS)	0.06	0.13
^{12}C (FB)	0.08	0.17
^{197}Au	0.15	0.30

equal to A . 2) The total charge of the nucleus must be fixed. Thus, the sum of the charges (contributed only by proton components) is equal to Z . In addition, a further natural assumption is made. 3) The number of p (or n, pn, nn etc.)-type clusters must be proportional to the number of protons (or number of neutrons, number of protons times the number of neutrons, number of neutrons squared etc.) in the nucleus. In this work clusters only up to 4th order will be considered. The highest order clusters, containing 12 valence quarks, will be assigned an effective probability to occur equal to $f_4 = 1 - f_1 - f_2 - f_3$ and generic parton distributions (see next section). In order to accommodate for this truncation, the nucleus must be treated as having an effective mass number $A' = A(1 - f_4)$ and an effective atomic number $Z' = Z(1 - f_4)$. These equations guarantee mass and charge conservation. Then the numbers of 1st, 2nd and 3rd-order clusters of all the possible types can be calculated solving a linear system of 10 equations, resulting in

$$n_p = \frac{f_1 Z'}{1 + f_2 + 2f_3}, \quad n_n = \frac{f_1 N'}{1 + f_2 + 2f_3}, \quad (1.1)$$

$$n_{pp} = \frac{f_2 Z'^2}{(1 + f_2 + 2f_3)(N' + Z')}, \quad n_{pn} = \frac{2f_2 Z'N'}{(1 + f_2 + 2f_3)(N' + Z')}, \quad (1.2)$$

$$n_{nn} = \frac{f_2 N'^2}{(1 + f_2 + 2f_3)(N' + Z')},$$

$$n_{ppp} = \frac{f_3 Z'^3}{(1 + f_2 + 2f_3)(Z' + N')^2}, \quad n_{ppn} = \frac{3f_3 Z'^2 N'}{(1 + f_2 + 2f_3)(Z' + N')^2}, \quad (1.3a)$$

$$n_{pnn} = \frac{3f_3 Z'N'^2}{(1 + f_2 + 2f_3)(Z' + N')^2}, \quad n_{nnn} = \frac{f_3 N'^3}{(1 + f_2 + 2f_3)(Z' + N')^2}, \quad (1.3b)$$

$$n_4 = \frac{A - n_1 - 2n_2 - 3n_3}{4}. \quad (1.4)$$

Here the notation is self-explanatory. For example, n_{pnn} indicates the number of 3rd-order clusters of the type containing one proton and two neutrons. The effective number of neutrons is $N' = A' - Z'$. Also n_1 , n_2 , n_3 and n_4 are the total number of clusters for 1st, 2nd, 3rd and 4th order. The last equation involves the real mass number A . The 4th-order clusters are not separated into various possible types.

5. Parton Distributions in Clusters

The parton distributions in nucleons or higher-order clusters describe the probability that a certain type of parton (valence or ocean quark or gluon) carries a certain fraction of the cluster momentum in a reference frame where the (longitudinal) momentum of the nucleus is very large. In this case motion is essentially one-dimensional and the transverse components of the parton momentum are usually and legitimately neglected. The momentum fraction for single nucleons (1st-order clusters) is defined as the Bjorken- x (x_{Bjorken}) and ranges from 0 to 1.

For 2nd, 3rd or higher-order clusters the upper limit of the momentum fraction is 2, 3 or more, relative to single nucleons as a parton can carry up to 2, 3, or more times the nucleon momentum. The parton distributions in general also depend on the 4-momentum exchanged between the probe (lepton or quark) and the parton, denoted as Q^2 . This is the invariant mass of the exchange quantum, be it a photon or gluon or an intermediate vector boson. However, when Q^2 is large, in excess of 2 GeV², this dependence becomes very weak, a phenomenon known as Q^2 -scaling. The phenomena discussed in this article originate in the Q^2 -scaling region, thus the distributions used will depend only on x_{Bjorken} . Scaling violations are relevant at very small x_{Bjorken} [22] [23] [27] [28] [29]. The calculations in this article intend to interpret data in the region $x_{\text{Bjorken}} > 1$ where the presence of higher-order clusters becomes prevalent. In the equations that follow x refers to the parton momentum fraction relative to the cluster in which the parton is found. Therefore, it is equal to $x_{\text{Bjorken}}/2$ for 2nd-order clusters, $x_{\text{Bjorken}}/3$ for 3rd-order and $x_{\text{Bjorken}}/4$ for 4th-order ones.

Inside clusters there are valence quarks, ocean (or sea) quarks with equal numbers of ocean antiquarks and gluons. In order to determine the parameters of the parton distributions certain constraints must apply. 1) Since the number of valence quarks of each flavor is fixed, the valence distributions should be normalized to this number. 2) The total momentum fractions carried by all partons must add up to the momentum of the cluster. Additional model assumptions are also needed. 3) The gluon to total-ocean momentum ratio is fixed at 1/5. 4) The strange quark distribution in the ocean is chosen to carry one half of the up-quark (or antiquark) ocean distribution. Naturally the antiquark distributions in the ocean are the same as those of the ocean quarks of the same flavor. The parton momentum distributions, *i.e.*, the probability distributions multiplied by x are assumed to have the following forms:

$$V^{u,d}(x) = B^{u,d} \sqrt{x} (1-x)^{b^{u,d}} \quad (\text{valence up and down quarks}), \quad (2.1)$$

$$S(x) = A(1-x)^a \quad (\text{sea quarks or antiquarks, one flavor}), \quad (2.2)$$

$$G(x) = C(1-x)^c \quad (\text{total gluon}), \quad (2.3)$$

where A , $B^{u,d}$ and C are constants. For the valence exponents, $b^d = b^u + 1$ as supported by scattering data [Ref]. If the total momentum fraction carried by one ocean quark flavor is x^s and that carried by the gluons is x^g then $A = x^s(1+a)$ and $C = x^g(1+c)$. This generic notation applies to clusters of all orders.

Isospin relations connect the distributions in various types of clusters of the same order.

$$V_p^u(x) = V_n^d(x), \quad (2.4a)$$

$$V_{pp}^u(x) = V_{nn}^d(x), \quad V_{pn}^u(x) = V_{pn}^d(x) = \frac{1}{2} [V_{pp}^u(x) + V_{pp}^d(x)], \quad (2.4b)$$

$$V_{ppn}^u(x) = V_{pnn}^d(x) = \frac{5}{2} \left[\frac{1}{6} V_{ppp}^u(x) + \frac{1}{3} V_{ppp}^d(x) \right], \quad (2.4c)$$

$$V_{ppn}^d(x) = V_{pmn}^u(x) = 2 \left[\frac{1}{6} V_{ppp}^u(x) + \frac{1}{3} V_{ppp}^d(x) \right]. \tag{2.4d}$$

The ocean and gluon distributions are the same in all types of clusters of the same order. The exponents of $(1 - x)$ in these distributions determine their overall behavior. Specifically, the higher the exponent, the “softer”, *i.e.*, more concentrated towards lower x the distribution is. The choice of exponents is guided by the DIS data themselves. It turned out that the specific values of ocean and gluon exponents for 3rd and higher-order clusters are not as essential as is the actual presence of such clusters in cross-section calculations. Even though to a first approximation the gluon distributions do not enter the calculations of DIS of electrons off nuclei, the gluon distributions have to be considered because they affect the total momentum ratios carried by ocean quarks. The exponents for proton-like clusters that produce the best fits to the EMC and QES data (to be discussed) are shown in **Table 2**. The exponents in other types of clusters of the same order are determined by the isospin relations. For valence, the exponents related to up quarks are given. For valence down quarks the exponents are simply increased by one unit.

Application of the above mentioned constraints and isospin relations yields the multiplicative constants that appear in the distributions. The calculations involve extensive use of Beta-functions. The results are shown in **Table 3** for proton-like clusters. For the ocean and gluon distributions the total momentum fraction is presented as it is proportional to the respective coefficient. The isospin relations determine the coefficients in all other types of clusters of all orders. In the case of 4th-order clusters the up and down valence quark distributions are taken to be the same. It may be worth noting that the ocean and gluon total

Table 2. Exponents of parton distributions in proton-like clusters. The exponents in other types of clusters of the same order are determined by the isospin relations. For 4th-order clusters the valence distribution is generic.

	P	PP	PPP	PPPP
Up-Valence (<i>b</i>)	3	9	15	21
Ocean (<i>a</i>)	9	11	18	23
Gluon (<i>c</i>)	6	10	16	20

Table 3. Coefficients in parton distributions for all orders of proton-like clusters used. The momentum fraction for the ocean pertains to one up quark or antiquark flavor. The 4th-order valence distributions are generic so that the up and down coefficients are the same.

	1st-order	2nd-order	3rd-order	4th-order
B^u (valence u-quark)	2.18750	7.04788	13.43519	31.57550
B^d (valence d-quark)	1.23046	3.70014	6.92752	31.57550
x^s (ocean, one flavor)	0.02289	0.02409	0.02442	0.02444
x^g (total gluon)	0.57239	0.60214	0.61039	0.61111

momentum fractions become saturated as the order of clusters increases.

6. Rescaled Bjorken-x

In a nucleus the physical size of bound nucleons (RMS radius of their wavefunction) may be slightly altered compared to free nucleons [30] [31]. This is due to the attraction from surrounding nucleons and it increases their size. This phenomenon clearly affects correlations as it increases the probability for cluster formation amounting to an effective decrease in the critical radius. Furthermore, it results in a decrease of the parton momentum fraction in bound nucleons or higher-order clusters, relative to “free” ones. It can be accounted for by rescaling x_{Bjorken} by a factor η :

$$x_{\text{bound}} = \eta x_{\text{free}} \quad (\eta < 1), \tag{3}$$

where η is a constant parameter that does not appreciably depend on the energy scale.

7. Structure Functions of Nuclei

The structure function of a nucleus with mass number A and atomic number Z is defined as the sum of all quark momentum distributions over all nucleons and higher-order clusters multiplied by the square of the charge of the quark. It is denoted by $F_2^{(A,Z)}(x)$, $x = x_{\text{Bjorken}}$.

The presence of correlations, described here as clusters, modifies the structure function relative to the one calculated for uncorrelated nucleons. The forms of the distribution functions are given by Eqs. (2.1, 2.2 and 2.3). In the construction of the structure function the cluster numbers, strange-to-up quark ocean ratios and isospin relations are employed to express the result in terms of only proton-like distributions. A straightforward calculation, thus, yields:

$$F_2^{(A,Z)}(x) = \frac{4}{9}V_{A,Z}^u(x) + \frac{1}{9}V_{A,Z}^d(x) + \frac{11}{9}S_{A,Z}(x), \tag{4.1}$$

where the total up ($V_{A,Z}^u$) down ($V_{A,Z}^d$) valence quark and ocean ($S_{A,Z}$) contributions are

$$\begin{aligned} V_{A,Z}^u(x) = & n_p V_p^u(x) + n_n V_p^d(x) + n_{pp} V_{pp}^u(x) + n_{pn} \frac{1}{2} [V_{pp}^u(y) + V_{pp}^d(y)] \\ & + n_{nn} V_{pp}^d(y) + n_{ppp} V_{ppp}^u(z) + n_{ppn} \frac{5}{2} \left[\frac{1}{6} V_{ppp}^u(z) + \frac{1}{3} V_{ppp}^d(z) \right] \\ & + n_{pnn} \left[\frac{1}{3} V_{ppp}^u(z) + \frac{2}{3} V_{ppp}^d(z) \right] + n_{nnn} V_{ppp}^d(z) + n_4 V_{pppp}^u(w), \end{aligned} \tag{4.2}$$

$$\begin{aligned} V_{A,Z}^d(x) = & n_p V_p^d(x) + n_n V_p^u(x) + n_{pp} V_{pp}^d(x) + n_{pn} \frac{1}{2} [V_{pp}^u(y) + V_{pp}^d(y)] \\ & + n_{nn} V_{pp}^u(y) + n_{ppp} V_{ppp}^d(z) + n_{ppn} \left[\frac{1}{3} V_{ppp}^u(z) + \frac{2}{3} V_{ppp}^d(z) \right] \\ & + n_{pnn} \frac{5}{2} \left[\frac{1}{6} V_{ppp}^u(z) + \frac{1}{3} V_{ppp}^d(z) \right] + n_{nnn} V_{ppp}^u(z) + n_4 V_{pppp}^u(w), \end{aligned} \tag{4.3}$$

$$S_{A,Z}(x) = n_1 S_p(x) + n_2 S_{pp}(y) + n_3 S_{ppp}(z) + n_4 S_{pppp}(w), \quad (4.4)$$

and $y = x/2$, $z = x/3$ and $w = x/4$. In Equation (4) the variable x is the Bjorken- x rescaled by the parameter η .

8. Heavy-to-Light Nuclei Cross-Section Ratios

The interaction investigated in this work is Deep Inelastic Scattering (DIS) of electrons off nuclei in the Q^2 -scaling region. The scattering cross section is proportional to the structure function. Therefore, the ratio of structure functions per nucleon for heavy over light nuclei studied as a function of x_{Bjorken} can reveal the presence and nature of correlations. Formally,

$$R(x) = \frac{F_2^{(A_1, Z_1)}(x)/A_1}{F_2^{(A_2, Z_2)}(x)/A_2}. \quad (5)$$

This is the ratio that revealed the EMC-effect. If no correlations or other modifications are present it should be equal to 1 for all x . However, data have shown that there is a strong, non-monotonic dependence of R on x even in the region $0 < x < 1$. Newer data show that R is measurable beyond $x = 1$. A step-wise behavior as x increases by a unit is a strong indication that the cluster model predicts correlations in the nucleus.

9. Comparison with Data

The calculations presented here are compared with data from JLab Experiment E02-019. The experiment used a 5.75 GeV electron beam and reported results for high Q^2 . Final-state interactions are very small under this condition. To extract information on short-range correlations the data are focused on the QES region with cuts in the energy transfer imposed to remove DIS contributions. Therefore, the comparison may not be expected to be complete. However, the x_{Bjorken} -dependence of cross section ratios must be similar for the following reasons: First, the quark-cluster model strongly overlaps with the Fermi-motion model [8]. Second, the nature of the correlations should be the same in both QES and DIS cases. There are strong indications for this. According to Ref. [32] [33] there is a remarkably linear relation between the EMC effect which manifests itself in the DIS region for $x_{\text{Bjorken}} < 1$ and the short-range correlations. In fact the A -dependence of the EMC effect closely matches that of the correlations effect according to Jefferson Lab data [34]. Because of these observations a comparison of the model derived using parton-distributions in the asymptotically-free region with the data in the QES region is possible. The comparison should be focused around $x_{\text{Bjorken}} = 1$ to evaluate the rise of the cross-section ratio and on the plateau that follows it.

First the 2007 data are addressed [35]. The free parameters in the model are R_c and η . The values of these parameters that produced the best fits to the 2007 data for various nuclei are shown in **Table 4**. Remarkably η turned out to have almost the same value for all nuclei studied. This parameter effectively controls the $x_{\text{Bjor-}}$

k_{en} point at which the cross section ratio begins to rise.

The cluster formation probabilities for each order are shown in **Table 5** for the various nuclei studied. The values presented correspond to the critical radius shown in **Table 4**. The 4th-order probability is the cumulative value for all orders higher than the 3rd. In the model presented here even the dilute deuterium nucleus has a substantial probability for correlations.

In **Figure 5** the model calculations are compared with the experimental data from 2007. The curves represent the best obtained fits of the theoretical ratio, R , for four cases. It is immediately observed that the sharp rise of the data right after $x = 1$ is well described by the model. However, the dip around $x = 1$ is not. There is a pseudo-plateau in the data for $1 < x < 1.8$ that is almost followed by the curves. However, the shape of the data in the case of the ^{12}C over ^3He ratio is not reproduced well. It must be noted that the parameters used for each nucleus are maintained for all curves. A better fit to the ^{12}C over ^3He data would result in a worse fit to the ^{12}C over ^2H data. Overall the curves involving ^2H are closer to the data than those for ^3He . The experimental uncertainties in these plots are significant, though, and ^3He may be an unusual case.

The same experiment produced more detailed data published in 2012 [36]. Fitting the theoretical model to the new data with the two independent parameters, R_c and η , resulted in slightly different values, presented in **Table 6**. The resulting cluster formation probabilities are shown in **Table 7**. For ^{63}Cu , ^{12}C and ^3He a larger critical radius was needed with the same value of the rescaling parameter while for ^2H the rescaling parameter was smaller, equal to 0.76. Stronger correlations were, thus, found for these nuclei based on the 2012 data.

The fit to data in which ^2H is in the denominator of the ratio is better, as shown in **Figure 6**. It is clear, though, that the model overestimates the ratio at high x . This is to some extent the result of the truncation of the model to the 4th-order clusters but mostly of the fact that the denominator, pertaining to ^2H ,

Table 4. The critical radius R_c and the rescaling parameter η for the various nuclei studied. These values fit the data from E02-019 (2007) [35].

	^{63}Cu	^{12}C	^3He	^2H
R_c (fm)	0.75	1.20	1.50	1.40
η	0.80	0.80	0.80	0.80

Table 5. The cluster formation probabilities for the nuclei studied. They correspond to the critical radii shown in **Table 4**. These values fit the data from E02-019 (2007) [35].

	f_1	f_2	f_3	f_4
^{63}Cu	0.7549	0.1402	0.0512	0.0537
^{12}C	0.8148	0.1093	0.0438	0.0321
^3He	0.8564	0.1212	0.0224	-----
^2H	0.9176	0.0824	-----	-----

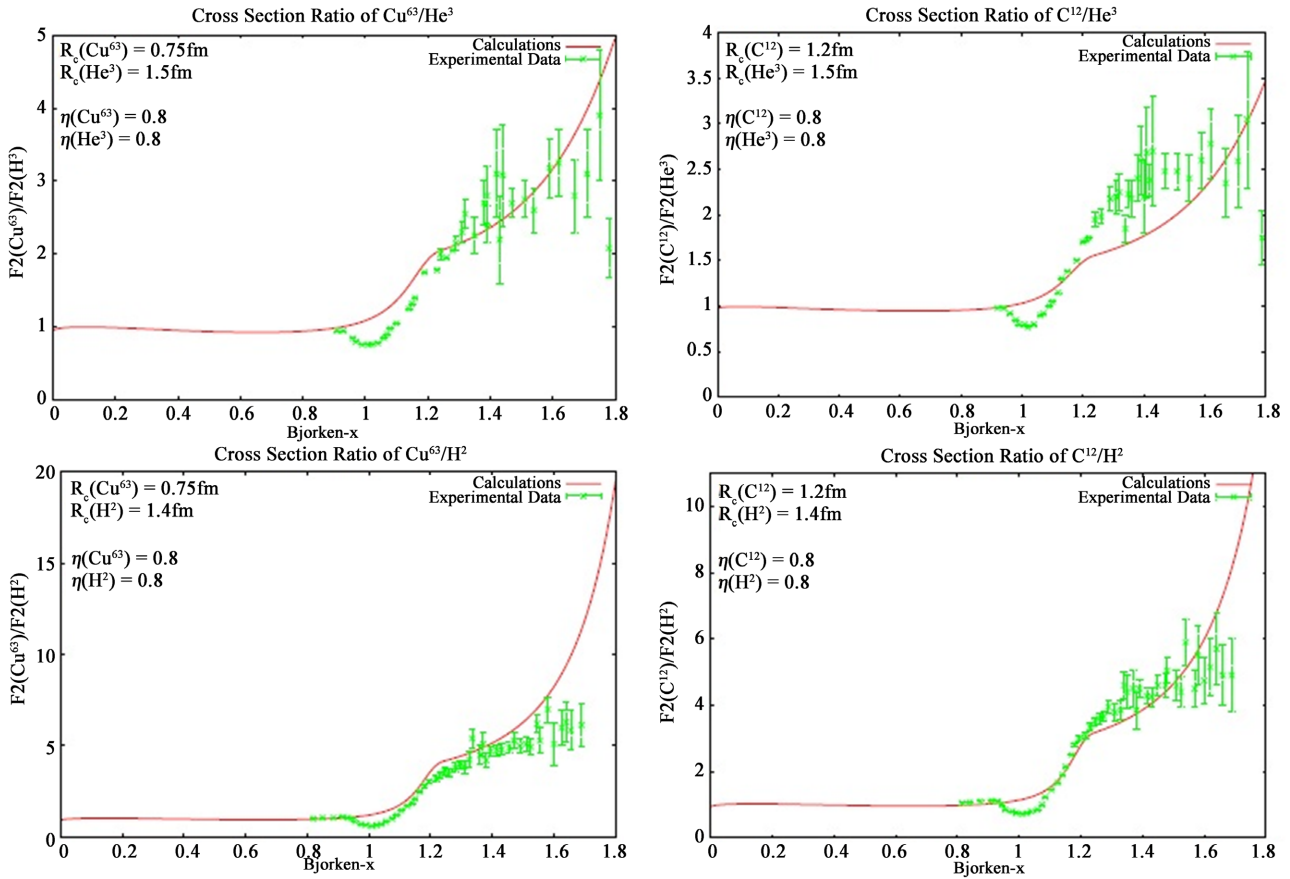


Figure 5. Comparison of the model calculations with data from E02-019 (2007) [35]. The nuclei involved are shown inside the plots. Upper left: $^{63}\text{Cu}/^3\text{He}$. Upper right: $^{12}\text{C}/^3\text{He}$. Lower left: $^{63}\text{Cu}/^2\text{H}$. Lower right: $^{12}\text{C}/^2\text{H}$. The model reproduces the sharp rise for $x > 1$ but fails to reproduce the dip at $x = 1$. The worst fit is for ^{12}C over ^3He data.

Table 6. The critical radius R_c and the rescaling parameter η for the various nuclei studied. These values fit the data from E02-019 (2012) [36].

	^{197}Au	^{63}Cu	^{12}C	^9Be	^4He	^3He	^2H
R_c (fm)	1.20	0.85	1.50	1.60	1.80	1.70	1.40
η	0.80	0.80	0.80	0.80	0.80	0.80	0.76

Table 7. The cluster formation probabilities for the nuclei studied. They correspond to the critical radii shown in Table 4. These values fit the data from E02-019 (2012) [36].

	f_1	f_2	f_3	f_4
^{197}Au	0.6772	0.1711	0.0704	0.0813
^{63}Cu	0.6960	0.1497	0.0629	0.0914
^{12}C	0.7151	0.1334	0.0597	0.0918
^9Be	0.7657	0.1179	0.0476	0.0688
^4He	0.7869	0.0741	0.0511	0.0879
^3He	0.7806	0.1692	0.0501	-----
^2H	0.9176	0.0824	-----	-----

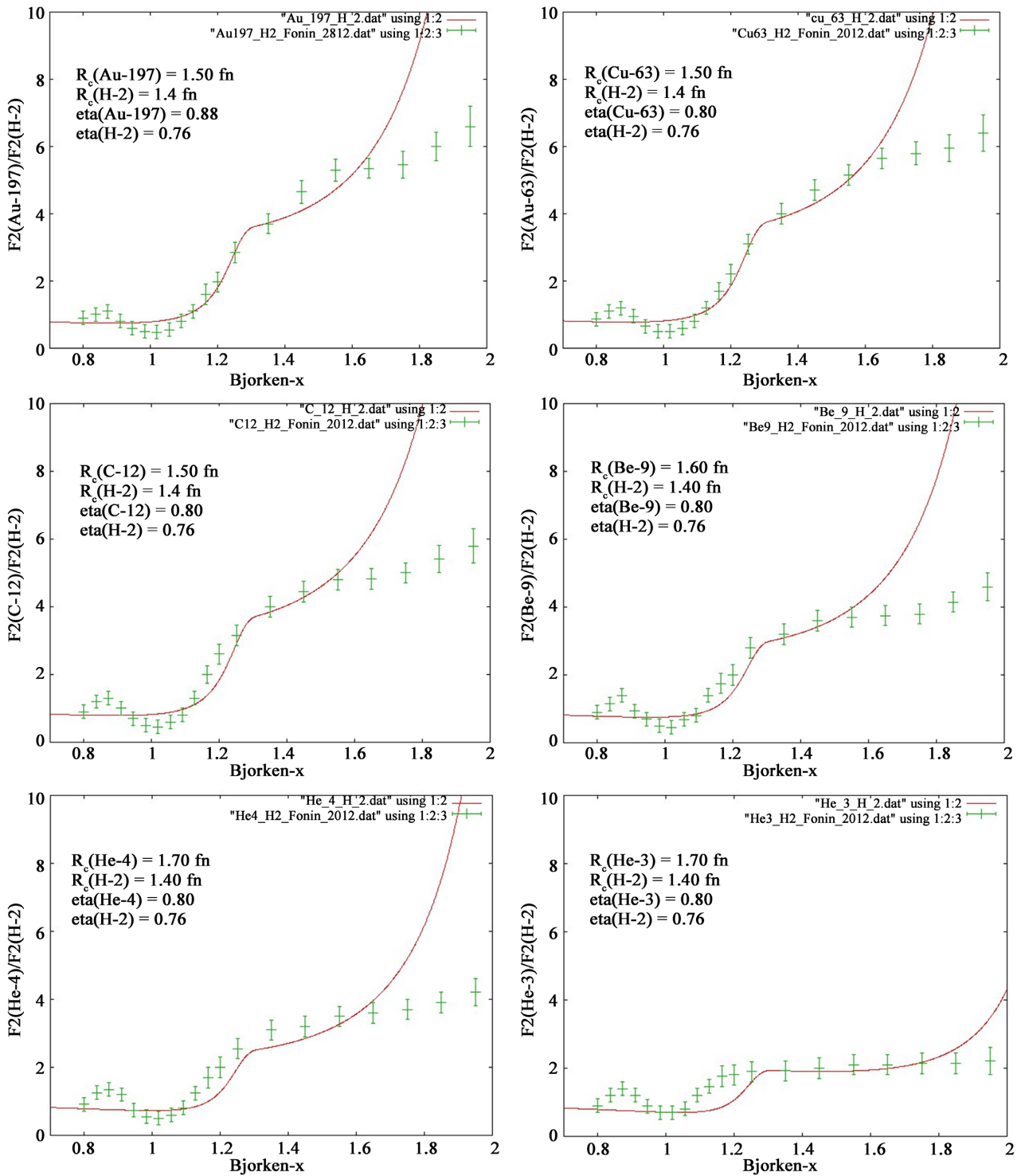


Figure 6. Comparison of the model calculations with data from E02-019 (2012) [36]. The nuclei involved are shown inside the plots. Upper left: $^{197}\text{Au}/^2\text{H}$. Upper right: $^{63}\text{Cu}/^2\text{H}$. Middle left: $^{12}\text{C}/^2\text{H}$. Middle right: $^9\text{Be}/^2\text{H}$. Lower left: $^4\text{He}/^2\text{H}$. Lower right: $^3\text{He}/^2\text{H}$. The model reproduces the sharp rise for $x > 1$.

approaches zero as x tends to 2 since there are no 3rd-order clusters in ^2H . The case of ^3He over ^2H ratio is most interesting in this regard. The level of the ^3He over ^2H plateau is described very well by the model as the curve remains flat up

to $x = 1.8$. This indicates that the 2nd-order correlations are accounted for successfully. Combined with the other results the flat-behavior of the data may imply the presence of another mechanism that extends the 2nd-order correlations possibly beyond $x = 2$ or that the data are inaccurate near the kinematic limits of the experiment. Alternatively the theoretical ratio should be lower at high x by allowing the parton distributions in clusters to be softer. This, however, would make it difficult to account for the exact slope of the rise at $x = 1$.

The differences in the critical radii used to fit the two sets of data merits some discussion. It must be pointed out that the fits are done over the entire sets of data so that the parameters for each nucleus are kept the same for the various nuclei ratios.

The observation that the two sets of data required slightly different values of the free parameters of the model, most importantly the critical radius that controls the strength of correlations, should be discussed. Clearly the data presented in 2007 carry substantially more uncertainty. Furthermore, there are differences in the average scattering angle of the emerging electron, *i.e.*, in the average Q^2 . The 2007 data used here correspond to an average $Q^2 = 4.1 \text{ GeV}^2$ while the data presented in 2012 are for $Q^2 = 1.5 \text{ GeV}^2$ and have the best kinematic range coverage and statistics. There may be a small scaling violation. The trends, however, are similar. As a result of these observations, the difference in the fitting parameters must result mostly from statistical differences in the data. The experiment has provided data for other scattering angles but with lower statistics. Members of the E02-019 Collaboration have elaborated on their measurements in Ref. [37].

An interesting extension and challenge is the comparison with data in the $2 < x < 3$ range. Such data were produced by the CLAS collaboration [38] and even though they are limited, they indicate the existence of a second plateau. The study of this range within the model is currently undertaken.

10. The Need for Many-Body Correlations

The existence of many-body correlations among bound nucleons is an irrefutable fact based on the data. To further elucidate this conclusion, the theoretical curves including 2nd, 3rd and 4th-order clusters are compared to 2007 data in **Figure 7**. The specific case of ^{63}Cu over ^3He is shown. It is clear that without up to 4th-order clusters the data cannot be reproduced. It is remarkable that even in the range $x < 2$ the higher-order correlations have a significant effect. The nucleon-nucleon clusters also affect the cross-section ratio for $x < 1$ but to a lesser extent.

11. Conclusion

In this work it was shown that many-body correlations in the nucleus are necessary in order to understand Quasi-Elastic Scattering (QES) data. This is in agreement with the need for such effects in Deep Inelastic Scattering (DIS) data.

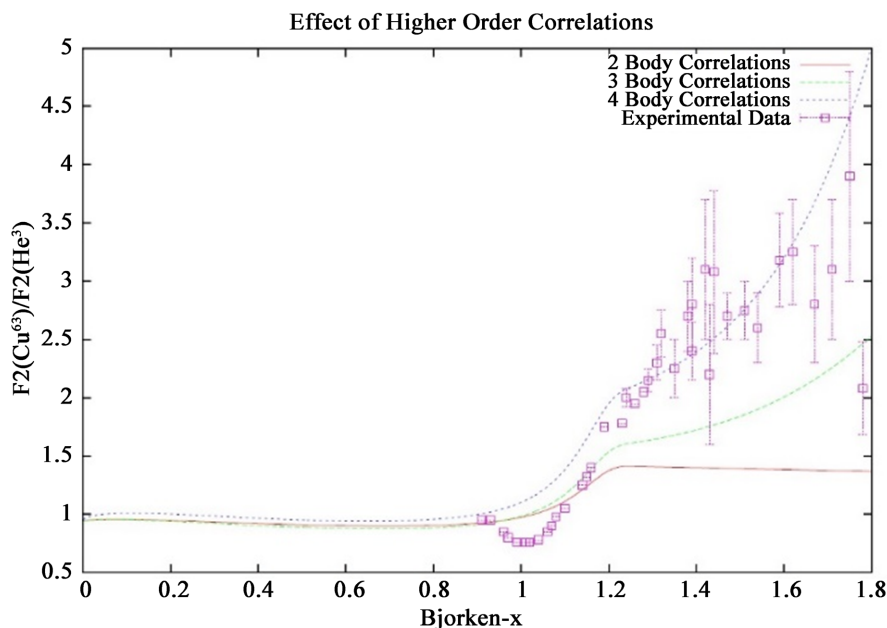


Figure 7. The ^{63}Cu to ^3He ratio. The curves correspond to theoretical calculations including 2nd (red), 3rd (green) and 4th (purple)-order clusters. The higher-order correlations are needed to reproduce the data for $1 < x < 2$. The data are from Ref. [35].

The nature of the correlations appears to be the same. A quark-cluster model has been constructed to account for these correlations. This assumes overlapping of bound-nucleon wave-functions to the extent that they share partons whose momentum distributions are consequently softened compared to those in independent nucleons. A network-based algorithm was developed in order to calculate the formation probabilities for all orders of clusters. This was supplemented by a model that produces the actual number of clusters of each type in every nucleus as well as a set of reasonable parton distributions. Comparison with two sets of data from Jefferson Laboratory helped extract the model parameters but the values obtained were slightly different for the two sets. The model generally reproduces the quasi-plateau in cross section ratios for $x_{\text{Bjorken}} > 1.0$ and the slope of the rising curve in the range $1.0 < x_{\text{Bjorken}} < 1.2$. Even in the studied region up to 4-body correlations are needed. The obvious next step is to study the extension of the model for $x_{\text{Bjorken}} > 2$. There are also data by the CLAS Collaboration to compare the theoretical calculations to [38]. However, certain questions arise. Is the coordinate-space network algorithm adequate to compute the cluster probabilities? So far it has given results that agree with data but the effect of relative momentum among nucleons can be considered. The small differences between parameters fitting the two sets of data may be attributable to different average Q^2 . Therefore, one can ask what is the exact Q^2 -dependence of many-body correlations? The similarity of the correlations between DIS and QES is intriguing but what would their mathematical formulation be if the parton-degrees of freedom are not entirely resolved? These questions are the subject of current and future investigations.

Conflicts of Interest

The authors declare no conflicts of interest regarding the publication of this paper.

References

- [1] EMC, Aubert, J.J., *et al.* (1983) *Physics Letters*, **123B**, 275.
- [2] Bodek, A., *et al.* (1983) *Physical Review Letters*, **50**, 1431. <https://doi.org/10.1103/PhysRevLett.50.1431>
- [3] Bodek, A., *et al.* (1983) *Physical Review Letters*, **51**, 534. <https://doi.org/10.1103/PhysRevLett.51.534>
- [4] EMC-NA38 Collaboration, Arneodo, M. *et al.* (1990) *Nuclear Physics*, **B333**, 1.
- [5] NMC Collaboration, Amaudriuz, P., *et al.* (1991) *Zeitschrift für Physik*, **51**, 387.
- [6] Kitagaki, T., *et al.* (1989) Results from FNAL E745 on Neutrino Nucleus Interactions (EMC Effect and Hadron Formation). *Proceedings of Electronuclear Physics with Internal Targets Conference*, Stanford, 95-115.
- [7] Bordalo, P., *et al.* (1987) *Physics Letters B*, **193**, 368-372. [https://doi.org/10.1016/0370-2693\(87\)91253-6](https://doi.org/10.1016/0370-2693(87)91253-6)
- [8] NA3 Collaboration, Badier, J., *et al.* (1983) *Zeitschrift für Physik*, **20**, 101-116. <https://doi.org/10.1007/BF01573213>
- [9] Alde, D.M., *et al.* (1991) *Physical Review Letters*, **66**, 133.
- [10] Kowitt, M.S., *et al.* (1994) *Physical Review Letters*, **72**, 1318.
- [11] Petridis, A., Lassila, K.E. and Vary, J.P. (1993) *Physical Review D*, **47**, 1906. <https://doi.org/10.1103/PhysRevD.47.1906>
- [12] Jalilian-Marian, J. (2005) *Nuclear Physics A*, **753**, 307-315. <https://doi.org/10.1016/j.nuclphysa.2005.02.156>
- [13] Betemps, M.A. and Gonçalves, V.P. (2008) *Journal of High Energy Physics*, **9**, 19. <https://doi.org/10.1088/1126-6708/2008/09/019>
- [14] Pirner, H.J. and Vary, J.P. (1981) *Physical Review Letters*, **46**, 1376. <https://doi.org/10.1103/PhysRevLett.46.1376>
- [15] Vary, J.P. (1984) *Nuclear Physics*, **418**, 195-214. [https://doi.org/10.1016/0375-9474\(84\)90550-5](https://doi.org/10.1016/0375-9474(84)90550-5)
- [16] Vary, J.P., Coon, S.A. and Pirner, H.J. (1985) Charge form Factors and Quark Clusters. *Proceedings of the International Conference on Hadronic Probes and Nuclear Interactions*, Tempe, 11-14 March 1985, 83-95.
- [17] Lassila, K.E. and Sukhatme, U.P. (1988) *Physics Letters B*, **209**, 343-346. [https://doi.org/10.1016/0370-2693\(88\)90959-8](https://doi.org/10.1016/0370-2693(88)90959-8)
- [18] Harindranath, A. and Vary, J.P. (1986) *Physical Review D*, **34**, 3378. <https://doi.org/10.1103/PhysRevD.34.3378>
- [19] Lassila, K.E., Petridis, A., Carlson, C. and Sukhatme, U.P. (1990) Multiquark Effects and Multiquark Fragmentation. *Proceedings of the Rice Meeting of the Division of Particles and Fields*, Houston, January 3-6 1990, 593.
- [20] Lassila, K.E., Sukhatme, U.P., Harindranath, A. and Vary, J.P. (1991) *Physical Review C*, **44**, 1188. <https://doi.org/10.1103/PhysRevC.44.1188>
- [21] Lassila, K.E., Petridis, A., Sukhatme, U.P. and Wilk, G. (1992) *Physics Letters B*, **297**, 191-196. [https://doi.org/10.1016/0370-2693\(92\)91091-M](https://doi.org/10.1016/0370-2693(92)91091-M)

- [22] Petridis, A. (1996) *Physical Review C*, **54**, 848.
<https://doi.org/10.1103/PhysRevC.54.848>
- [23] Petridis, A. (2018) *International Journal of Applied and Natural Sciences*, **7**, 75.
- [24] Pirner, H.J. and Vary, J.P. (2011) *Physical Review C*, **84**, 015201.
<https://doi.org/10.1103/PhysRevC.84.015201>
- [25] Reuter, W., et al. (1982) *Physical Review C*, **26**, 806.
<https://doi.org/10.1103/PhysRevC.26.806>
- [26] Anni, R., Co', G. and Pellegrino, P. (1995) *Nuclear Physics*, **584**, 35-59.
[https://doi.org/10.1016/0375-9474\(94\)00508-K](https://doi.org/10.1016/0375-9474(94)00508-K)
- [27] Gribov, L., Levin, E. and Ryskin, M. (1981) *Nuclear Physics*, **188**, 555-576.
[https://doi.org/10.1016/0550-3213\(81\)90007-9](https://doi.org/10.1016/0550-3213(81)90007-9)
- [28] Close, F.E., Qiu, J. and Roberts, R.G. (1989) *Physical Review D*, **40**, 2820.
<https://doi.org/10.1103/PhysRevD.40.2820>
- [29] Eskola, K., Qiu, J. and Wang, X.-N. (1994) *Physical Review Letters*, **72**, 36.
<https://doi.org/10.1103/PhysRevLett.72.36>
- [30] Li, G.L., Liu, K.F. and Brown, G.E. (1988) *Physics Letters B*, **213**, 531-536.
[https://doi.org/10.1016/0370-2693\(88\)91305-6](https://doi.org/10.1016/0370-2693(88)91305-6)
- [31] Close, F.E., Roberts, R.G. and Ross, G.G. (1984) *Physics Letters B*, **142**, 202-206.
[https://doi.org/10.1016/0370-2693\(84\)91262-0](https://doi.org/10.1016/0370-2693(84)91262-0)
- [32] Weinstein, L.B., Piasetzky, B.E., Higinbotham, D.W., Gomez, J., Hen, O. and Shneur, R. (2011) *Physical Review Letters*, **106**, 052301.
<https://doi.org/10.1103/PhysRevLett.106.052301>
- [33] Hen, O., Piasetzky, E. and Weinstein, L.B. (2012) *Physical Review C*, **85**, 047301.
<https://doi.org/10.1103/PhysRevC.85.047301>
- [34] Seely, J., et al. (2009) *Physical Review Letters*, **103**, 202301.
- [35] Fomin, N. (2007) arXiv: 0808.2625.
- [36] Fomin, N., et al. (2012) *Physical Review Letters*, **108**, 092502.
- [37] Arlington, J., et al. (2012) arXiv: 1206.6343.
- [38] CLAS Collaboration, Egiyan, K. S., et al. (2006) *Physical Review Letters*, **96**, 082501.